THE JOURNAL OF PHYSICAL CHEMISTRY C

Article

pubs.acs.org/JPCC

Structural, Spectroscopic, and Electronic Properties of Cubic G0-Rb_2KTiOF_5 Oxyfluoride

Victor V. Atuchin,[†] Ludmila I. Isaenko,[‡] Valery G. Kesler,[§] Lei Kang,[∥,#] Zheshuai Lin,*[,∥] Maxim S. Molokeev,[⊥] Alexander P. Yelisseyev,[‡] and Sergey A. Zhurkov[‡]

[†]Laboratory of Optical Materials and Structures, Institute of Semiconductor Physics, and [‡]Laboratory of Crystal Growth, Institute of Geology and Mineralogy, Siberian Branch of the Russian Academy of Sciences, Novosibirsk 630090, Russia

[§]Laboratory of Physical Bases of Integrated Microelectronics, Institute of Semiconductor Physics, Siberian Branch of the Russian Academy of Sciences, Novosibirsk 90, 630090, Russia

[∥]BCCRD, Key Laboratory of Functional Crystals and Laser Technology, Technical Institute of Physics and Chemistry, CAS, P.O. Box 2711, Beijing 100190, China

[⊥]Laboratory of Crystal Physics, Institute of Physics, Siberian Branch of the Russian Academy of Sciences, Krasnoyarsk 660036, Russia

[#]Graduate School of the Chinese Academy of Sciences, Beijing 100049, PR China

ABSTRACT: The G0-Rb_2KTiOF_5 single crystals with dimensions up to nearly a centimeter in size have been prepared by slow solidification method. The elpasolite-related crystal structure of G0-Rb_2KTiOF_5 has been refined by Rietveld method at T = 298 K (space group $Fm\bar{3}m$, Z = 4, a = 8.880(1) Å, V = 700.16(2) Å^3; R_B = 2.66%). The wide optical transparency range of 0.25−9 μm and forbidden band gap of E_g = 3.87 eV have been obtained for the G0-Rb_2KTiOF_5 crystal. Dominating photoluminescence bands at 3.36 and 2.33 eV are related to free and self-trapped excitons, respectively. The electronic structure of G0-Rb_2KTiOF_5 has been evaluated by X-ray photoelectron spectroscopy and calculated with the first-principles methods. A good agreement between theoretical and experimental results has been achieved. Chemical bonding effects have been discussed for all metal ions using binding energy difference parameters and a wide comparison with related oxides and fluorides. The competition between O^{2-} and F^- ions for metal valence electrons has been found.

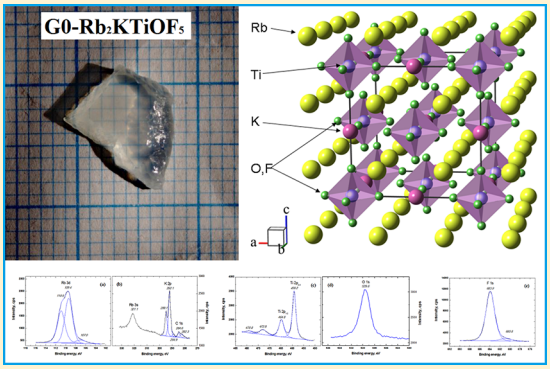

1. INTRODUCTION

Complex transition metal oxyfluorides are interesting materials because the strong distortion of metal-(O,F) polyhedra in a crystal lattice is achievable due to the different ionicity of metal-O and metal-F bonds. The anionic sublattices of these compounds are generally the $[MO_{6-x}F_x]$ (M = W, Mo, Nb, Ti; x = 3, 4, 5) octahedral groups.[1−7] At high temperature, usually, the anions are completely disordered and the cubic phase of oxyfluoride exists. As temperature decreases, the anions become more and more ordered. Thus, a set of phase transitions governed by the step-by-step anion ordering process is typically observed with the change of temperature, and highly ordered derivatives have been found in many oxyfluorides at low temperatures.[3,5,8−11] On the other hand, oxyfluorides are commonly synthesized in powder forms only because of great technological difficulties. Up to now, the millimeter-sized single crystals have been grown for only very few oxyfluorides, by which the measurements on the optical and electronic properties in crystals can be fulfilled at high accuracy.[12−20]

The oxyfluoride Rb_2KTiOF_5 attracts our attention since its structural feature is similar to that of $KTiOPO_4$,[21] a very important nonlinear optical material. In both crystals the titanium ions are in the octahedral environment with the acentric arrangements. The crystals of room-temperature modification G0-Rb_2KTiOF_5 are cubic, space group $Fm\bar{3}m$, Z = 4, with complete anion disorder.[1,22,23] At ∼215 K, the phase transition takes place to low-temperature tetragonal phase G1-Rb_2KTiOF_5, space group $I4/m$, Z = 10, and as large entropy variation as $\Delta S \approx R\ln 8$ was reported for the transition.[24,25] Here, the phase designation by Gi indices, where G0 is a parent high-temperature cubic phase of the compound and Gi (i = 1, 2, 3,..) are the low-symmetry phases formed sequentially on temperature decrease, is used. Earlier, this notation was introduced for fluoride and oxyfluoride crystals with elpasolite-like structures.[26,27] Vibrational properties and chemical bonding effects in G0-Rb_2KTiOF_5 were explored using IR, Raman and NMR spectroscopy methods and density functional theory.[23,28−30] However, the accurate investigations on the optical parameters and electronic structure of this oxyfluoride are practically absent mainly due to the lack of a large crystal of

Received: February 7, 2013
Revised: March 15, 2013
Published: March 18, 2013

dx.doi.org/10.1021/jp401391y | J. Phys. Chem. C 2013, 117, 7269−7278

high quality. In present study, the centimeter-sized single crystals of G0-Rb_2KTiOF_5 are grown, and the measurements of absorption/luminescence and X-ray photoelectron spectra, and the first-principles calculations on the electronic band structure are reported. The chemical bonding effects, appeared due to the mixed O/F anion system, are explored using core level XPS and compared to those in the previously measured $K_3WO_3F_3$ and $CsMnMoO_3F_3$ where O/F = 1.[18,31,32] In G0-Rb_2KTiOF_5, ratio O/F = 0.2 is noticeably lower and new features are supposed.

2. EXPERIMENTAL METHODS

Synthesis. The synthesis of Rb_2KTiOF_5 was carried out based on the following reaction

$$K_2TiF_6 + TiO_2 + 4RbF = 2Rb_2KTiOF_5$$

where special precautions are needed to avoid reagent hydration and keep the O/F stoichiometry.[31−33] High-purity K_2CO_3, Rb_2CO_3, TiO_2, NH_4F (all 99.9%, CJSC "Plant of rare metals", Russia) and aqueous hydrofluoric acid (HF) (48% HF in weight, CJSC "Plant of rare metals", Russia) were used as initial reagents. Titanium oxide was fired during 4 h in a platinum crucible at 800 °C in the air to remove residual water. The water-free RbF was formed from Rb_2CO_3 by neutralization of HF and evaporation of the formed solution at the acid excess. The synthesis of K_2TiF_6 was carried out in two stages. In the first stage, the powders of K_2CO_3 and TiO_2 taken in stoichiometric proportion were alloyed at 1000 °C with a potassium titanate formation. After cooling, the obtained alloy was ground in a ceramic vessel and placed into a Teflon vessel. Afterward, concentrated etching acid was added by small portions to produce the relatively violent exothermic reaction

$$K_2TiO_3 + 6HF = K_2TiF_6 + 3H_2O\uparrow$$

Then, the K_2TiF_6 was recrystallized adding some amount of HF and the crystals were washed in cold distilled water.

Single-Crystal Growth. The G0-Rb_2KTiOF_5 crystals were grown by slow solidification method. The obtained chemicals of K_2TiF_6, TiO_2, and RbF were mixed in a stoichiometric ratio and placed in a platinum crucible covered by a platinum sleeve which was continuously blown through with dry nitrogen in a growth furnace. The furnace was heated at the rate of 100 °C/h up to 1000 °C and kept at this temperature during 6 h. Afterward, the temperature was lowered at the rate of 5 °C/h during a day and then at the rate of 100 °C/h to room temperature. The single crystal blocks with dimensions up to nearly a centimeter size were selected from the solidified compound and used for structural and optical characterization. As an example, a big crystal of G0-Rb_2KTiOF_5 is shown in Figure 1.

Structure Determination. The X-ray single crystal data from Rb_2KTiOF_5 were measured by SMART APEXII diffractometer (Mo K_α, λ = 0.7106 Å) at room temperature. The matrix of orientation and cell parameters were calculated and refined by 121 reflections. The main information about crystal data, data collection and refinement are reported in Table 1. The X-ray data from Rb_2KTiOF_5 crystal were measured for the exposure time of 10 s on each frame. Each new frame was obtained by crystal rotation along ω-axis by 0.5° at the fixed φ angle. The ω value was increased from 0 to 182°. The 364 frames were measured at each fixed φ equal to 0, 120, and 240°. After that, the program APEXII from Bruker integrated the intensities of reflections. Space group $Fm\bar{3}m$ was defined by the analysis of extinction rules and intensity statistics

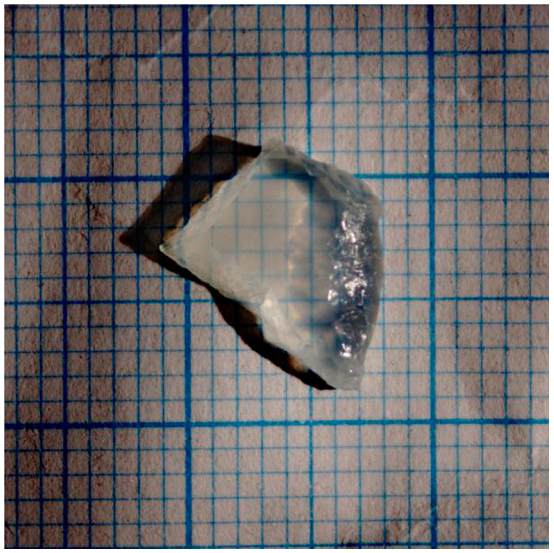

Figure 1. G0-Rb_2KTiOF_5 crystal grown by slow solidification method.

Table 1. Crystallographic Data and Main Parameters of Processing and Refinement of G0-Rb_2KTiOF_5

Crystal Data	
chemical formula	Rb_2KTiOF_5
M_r	368.94
space group, Z	$Fm\bar{3}m$, 4
a, (Å)	8.880(1)
V, (Å^3)	700.16(2)
D_x, Mg/m^3	3.500
μ, mm^{-1}	15.65
size	0.2 × 0.2 × 0.2 mm
Data Collection	
wavelength	MoK_α, λ = 0.7106 Å
measured reflections	1671
independent reflections	74
reflections with $I > 2\sigma(I)$	62
absorption correction	multiscan
R_{int}	0.0469
$2\theta_{max}$ (°)	59.13
h	−11 → 11
k	−12 → 12
l	−11 → 12
Refinement	
$R[F^2 > 2\sigma(F^2)]$	0.0266
$wR(F^2)$	0.0907
S	1.012
weight	$w = 1/[\sigma^2(F_o^2) + (0.0382P)^2 + 25P]$ where $P = \max(F_o^2+2F_c^2)/3$
$(\Delta/\sigma)_{max}$	<0.06
$\Delta\rho_{max}$, e/Å^3	0.67
$\Delta\rho_{min}$, e/Å^3	−1.01
extinction correction coefficient (SHELX97)	0.0018(8)

obtained from all reflections. Multiscan absorption correction of reflection intensities was performed by APEXII software. Then, the intensities of equivalent reflections were averaged. The structure of Rb_2KTiOF_5 was solved by direct methods using the SHELXS program.[34] The coordinates of all atoms were determined. The structure refinement was carried out by least-squares minimization in SHELXL97.[35] The atoms of O

dx.doi.org/10.1021/jp401391y | J. Phys. Chem. C 2013, 117, 7269−7278

and F were refined with the same coordinates and equal thermal parameters. Thermal parameters of all atoms were refined anisotropically.

Absorption/Luminescence Spectroscopy. Absorption/luminescence spectra were measured for the crystal plates. The plates were cut and polished without crystallographic orientation control. Optical transmission/absorption measurements were produced using a UV-2501PC Shimadzu spectrometer in the UV to near IR region and a Fourier transform spectrometer Infralum FT-801 in the mid-IR. Absorption coefficients were calculated from transmission measurements in the transparency region with the use of the following formula[36]

$$T = \frac{(1-R)^2 e^{-\alpha d}}{(1-R^2 e^{-2\alpha d})} \quad (1)$$

where α is the absorption coefficient (cm^{-1}), d is the sample thickness (cm), and R is the power reflection coefficient per surface. The maximum transmission level allows one to estimate roughly refraction index n and reflection index R, as well as to calculate α. An attempt has been made to determine the dominant mechanism of band-to-band electronic transitions. The kind of transition can be defined from the functional relationship between absorption α and photon energy $h\nu$.[36] Thus, for direct-allowed and indirect-allowed transitions, relations $\alpha h\nu \propto (h\nu - E_g)^{1/2}$ and $\alpha h\nu \propto (h\nu - E_g)^2$ are fulfilled, respectively. The estimations were carried out for a 0.85 mm thick G0-Rb_2KTiOF_5 plate. Band gap values E_g were estimated by extrapolating the linear part of the $(\alpha h\nu)^2$ versus $h\nu$ or $(\alpha h\nu)^{1/2}$ versus $h\nu$ curves to $\alpha(h\nu) = 0$. The photoluminescence (PL) spectra were recorded at 300 K using a diffraction luminescence spectrometer SDL1 and FEU100 photomultiplier as a detector. In spectral range from 270 to 600 nm the PL was excited by the 1 kW Xe lamp whereas a proper excitation wavelength was separated using a MDR2 diffraction monochromator.

X-ray Photoelectron Spectroscopy. Observation of the G0-Rb_2KTiOF_5 electronic structure was produced using surface analysis center SSC (Riber) with the X-ray photoelectron spectroscopy (XPS) method. Several millimeter-sized crystals were selected and gently ground up to the formation of fine powder. Then, the powder was pressed into a freshly prepared indium foil taken as a substrate and inserted into the vacuum chamber of XPS device. The nonmonochromatic Al Kα radiation (1486.6 eV), with the power source of 300 W, was used for the photoemission excitation. The energy resolution of the instrument was chosen to be 0.7 eV, so as to have a sufficiently small broadening of natural core level lines at a reasonable signal-noise ratio. Under the conditions, the observed full width at half-maximum (fwhm) of the Au $4f_{7/2}$ line was 1.31 eV. The binding energy (BE) scale was calibrated in the reference to Cu $3p_{3/2}$ (75.1 eV) and Cu $2p_{3/2}$ (932.7 eV) lines, assuring the accuracy of 0.1 eV in any peak energy position determination. The photoelectron energy drift due to charging effects was taken into account in reference to the position of the C 1s (284.8 eV) line generated by adventitious carbon present on the surface of the powder as-inserted into the vacuum chamber. Chemical composition is defined using the detailed spectra of Rb 3d, K $3p_{3/2}$, Ti $2p_{3/2}$, O 1s, and F 1s core levels and the known element sensitivity factors.[37]

3. COMPUTATIONAL METHODS

The first-principles calculations for the G0-Rb_2KTiOF_5 crystal are performed by the plane-wave pseudopotential method[38] implemented in the CASTEP package[39] based on the density functional theory (DFT).[40] The ion-electron interactions are modeled by the optimized normal-conserving pseudopotentials for all constituent elements, and the O $2s^22p^4$, F $2s^22p^5$, K $3s^23p^64s^1$, Ti $3d^24s^2$, and Rb $4s^24p^65s^1$ electrons are treated as the valence electrons, respectively.[41,42] The Perdew, Burke, and Ernzerhof (PBE)[43] exchange-correlation functional of generalized gradient approximation (GGA)[44] with a high kinetic energy cutoff of 900 eV and fine Monkhorst-Pack k-point meshes[45] with the spanning of less than 0.04/Å^3 in the Brillouin zone is adopted for the calculations. Meanwhile, the virtual crystal approximation (VCA)[46] is adopted to take into account the weight average of the potential of each atomic species, because the occupancies for some atoms are statistically distributed in the G0-Rb_2KTiOF_5 crystal. Our tests reveal that the above computational set ups are sufficiently accurate for the present purposes.

4. RESULTS AND DISCUSSION

The crystal structure of cubic G0-Rb_2KTiOF_5 was found and refined previously.[22,23] In ref 23, the model of crystal structure was proposed, where two mixed disordered O/F positions 24e and 96j were assumed. The thermal parameters of atoms (O/F)1 and (O/F)2 were anisotropic. This approach provides two different bond lengths, d(Ti-(O/F)1) = 1.914(1)Å and d(Ti-(O/F)2) = 1.872(7) Å, and the refinement leads to as low R-factor as R_B = 2.08%. In present study, we follow the model proposed in ref 22, where unique mixed disordered O/F position 24e was considered with the anisotropic thermal parameter. Up to now, there is no clear physical evidence to specify several different anion positions in cubic G0-Rb_2KTiOF_5.[1,22−25,30] As a result, the structure was finally refined with as small R-factor as R_B = 2.66% also (Table 1). The cell parameters reported for G0-Rb_2KTiOF_5 are a bit different: (1) a = 8.9002(1) Å;[22] (2) a = 8.8675(6) Å;[23] (3) a = 8.880(1) Å (Table 1) and the scattering may indicate some difference in the composition or vacancies in the structure. The coordinates of atoms, thermal parameters, and occupancies are given in Table 2. The crystal structure of G0-Rb_2KTiOF_5 elpasolite is shown in Figure 2.[22,47] The parent phase G0-Rb_2KTiOF_5 shows elpasolite-like structure (distorted perovskite). The cations Ti^{4+}, K^+, and Rb^+ are coordinated by 6, 6, and 12 anions, respectively. The F^- and O^{2-} anions occupy one mixed position 24e. This position is coordinated by four Rb^+ ions, one Ti^{4+} ion, and one K^+ ion. The main interatomic distances are 1.8979(3), 3.1559(3), and 2.5420(3) Å for Ti−O(F), Rb−O(F), and K−O(F), respectively. Despite the difference in unit

Table 2. Coordinates of Atoms, Occupancy (q), and Thermal Parameters (U) of G0-Rb_2KTiOF_5

atom	X	Y	Z	q	U, Å^2
Ti	0	0	0	1	$U_{11} = U_{22} = U_{33}$ = 0.0163(9)
Rb	1/4	1/4	1/4	1	$U_{11} = U_{22} = U_{33}$ = 0.0311(8)
K	1/2	0	0	1	$U_{11} = U_{22} = U_{33}$ = 0.021(1)
F	0.2121(9)	0	0	5/6	U_{11} = 0.017(3)
					$U_{22} = U_{33}$ = 0.065(3)
O	0.2121(9)	0	0	1/6	U_{11} = 0.017(3)
					$U_{22} = U_{33}$ = 0.065(3)

dx.doi.org/10.1021/jp401391y | J. Phys. Chem. C 2013, 117, 7269−7278

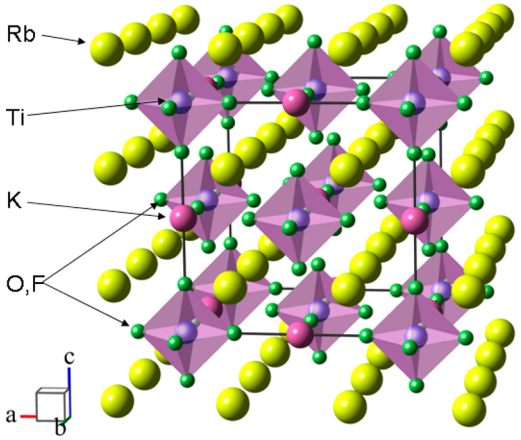

Figure 2. Crystal structure of G0-Rb_2KTiOF_5. Unit cell is outlined. Lone fluorine and oxygen atoms are omitted for clarity.

cell parameters, bond length d(O/F) = 1.8979(3)Å is intermediate between the lengths d(Ti-(O/F)1) and d(Ti-(O/F)2) found in ref 22 and is close to average bond length d(Ti−F) = 1.901 Å in fluorides[48] because of low ratio O/F = 0.2 in G0-Rb_2KTiOF_5.

As shown in Figure 3, the transparency range for the $RbKTiOF_5$ plate 0.85 mm thick covers the 0.31−9.0 μm range

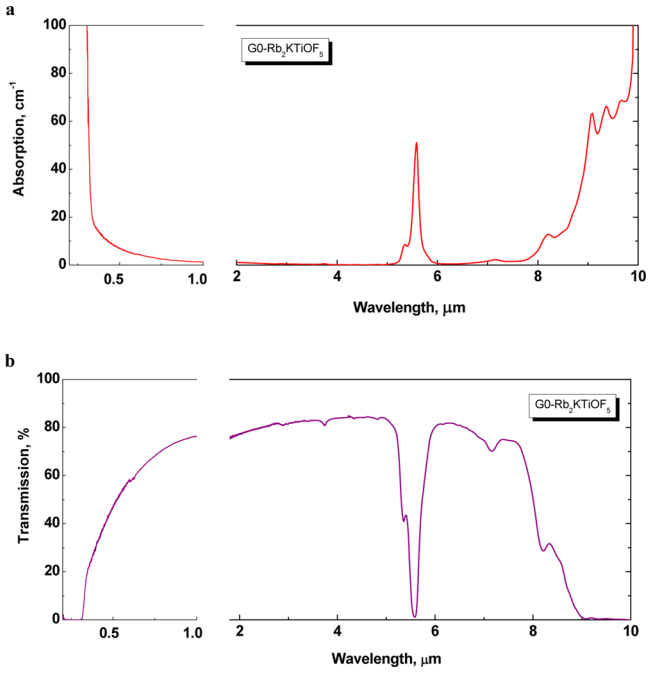

Figure 3. (a) Transmission and (b) absorption spectra recorded from G0-$RbKTiOF_5$ crystal plate with the thickness of 0.85 mm at T = 300 K.

on the 5% level at 300 K. The shortwave absorption edge is determined by the band gap, whereas the second and third harmonics from lattice vibrations are responsible for the longwave limit. An intense absorption peak is observed at 5.58 μm. The fundamental absorption at λ < 0.343 μm gives a direct line in coordinates $(\alpha^*h\nu)^2 = f(h\nu)$ (Figure 4), which corresponds to the case of direct allowed electronic transition between the valence and conduction bands. The band gap was estimated to be E_g = 3.87 eV at T = 300 K. Maximal

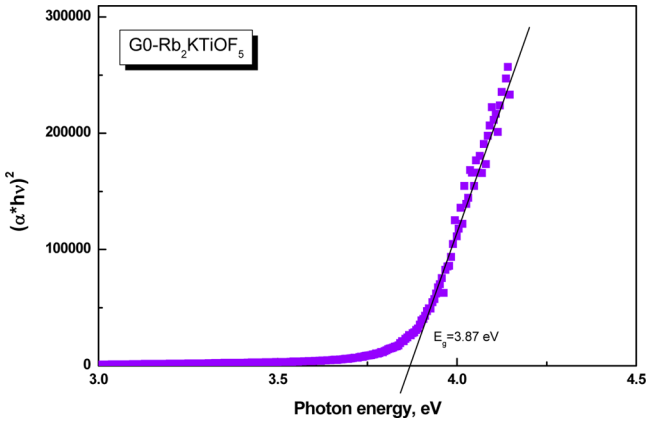

Figure 4. Absorption spectrum plotted in coordinates of $(\alpha^*h\nu)^2 = f(h\nu)$ at T = 300 K. Optical band gap is E_g = 3.87 eV for direct allowed electronic transitions.

transmission $T \sim 0.847$ is observed at the wavelengths near 5 μm in Figure 3b and refractive index n was estimated to be ~1.8 taking into account multiple reflections on the G0-Rb_2KTiOF_5 plate faces. The G0-Rb_2KTiOF_5 crystals exhibit a relatively intense photoluminescence (PL) at room temperature in comparison, for example, with $LiGaS_2$ where similar luminescence band was obtained.[49] PL spectra, recorded at 7 different excitation wavelengths in the 270−700 nm range, are shown in Figure 5. PL is excited most effectively near the fundamental

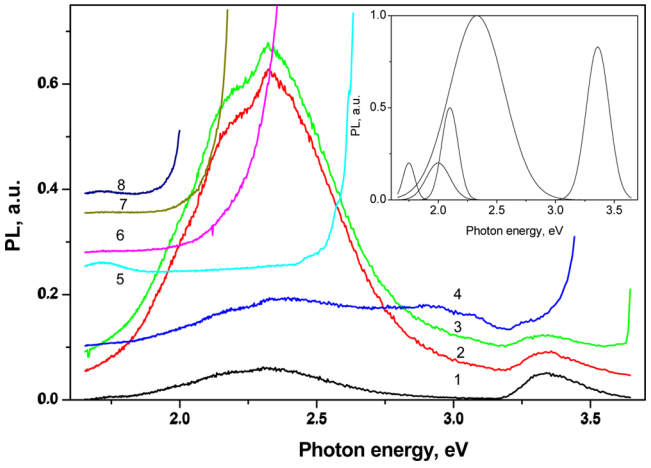

Figure 5. Photoluminescence spectra recorded from G0-$RbKTiOF_5$ at T = 300 K. The spectra are recorded under excitation at (1) 270 nm (4.59 eV), (2) 300 nm (4.098 eV), (3) 330 nm (3.756 eV), (4) 350 nm (3.54 eV), (5) 450 nm (2.73 eV), (6) 500 nm (2.479 eV), (7) 550 nm (2.253 eV), and (8) 600 nm (2.065 eV). The result of spectrum (1) decomposition into individual Gaussian components is shown in the insert.

absorption edge. PL spectra are complicated; most of them contain at least five components. Their large width (>0.12 eV) indicates a strong electron−phonon interaction. In such a case, the band shape is Gaussian. The decomposition result of spectrum (1) into individual Gaussian is given in the insert in Figure 5. The parameters of Gaussian components are given in Table 3. Two additional bands centered at 2.93 and 3.07 eV are observed at 3.54 eV excitation (spectrum (4) in Figure 5). The most intense PL band at 2.33 eV with full width at half-maximum (fwhm) = 0.56 eV is characterized by a relatively

dx.doi.org/10.1021/jp401391y | J. Phys. Chem. C 2013, 117, 7269−7278

Table 3. Parameters of Gauss Functions Used for Spectrum (1) Decomposition in the Insert in Figure 5

component	energy position, eV	fwhm, eV
1	3.36	0.23
2	2.33	0.56
3	2.1	0.17
4	2.0	0.24
5	1.75	0.12

large Stokes shift (absorption energy-emission energy ~1.5 eV) and the band may be related to self-trapped excitons (STE).[50] The shortwave PL band at 3.36 eV excited with $h\nu > E_g$ photons (behind the fundamental absorption edge) is likely associated with free excitons. The other PL bands can be due to native point defects in G0-Rb_2KTiOF_5 crystals; the most typical of them are anion vacancies (F-centers) and their complexes.

The survey photoemission spectrum of G0-Rb_2KTiOF_5 is shown in Figure 6. All the spectral features are attributed to the

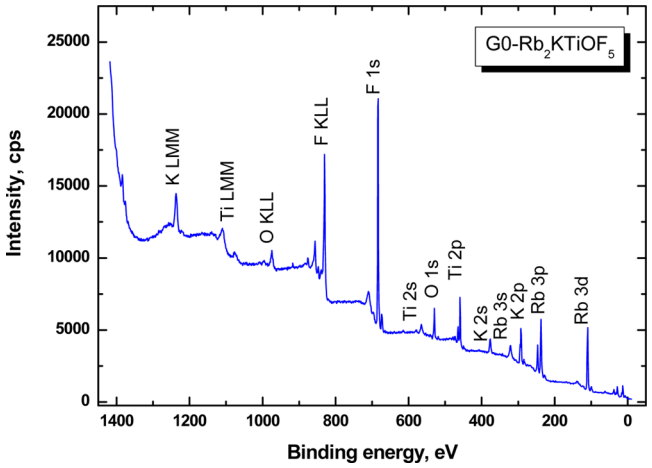

Figure 6. Survey photoemission spectrum from G0-Rb_2KTiOF_5.

constituent element core levels or Auger lines except for the C 1s line related to adventitious hydrocarbons adsorbed at the surface from the air. The total suite of BE values of spectral features recorded from G0-Rb_2KTiOF_5 is presented in Table 4 together with three related compounds measured previously using the same XPS device. From comparison, the BE(Rb 3d) in G0-Rb_2KTiOF_5 is a little higher than that in $RbTiOPO_4$ oxide. However, the BE(K $2p_{3/2}$) in G0-Rb_2KTiOF_5 is noticeably lower than those in $KTiOPO_4$ oxide and KWO_3F_3 oxyfluoride. As to Ti $2p_{3/2}$ core level, the BE(Ti $2p_{3/2}$) in G0-Rb_2KTiOF_5 is higher than those in $KTiOPO_4$-family oxides. So, it is impossible to see a clear bonding trend of K^+, Rb^+, and Ti^{4+} cations using BE values and a more detailed observation is needed. The representative constituent element core levels and doublets measured from G0-Rb_2KTiOF_5 are shown in Figure 7. In several lines, the weak intensity component has been detected at the higher BE side that may appear due to a differential charging effect. The chemical composition of the sample determined by XPS is Rb/K/Ti/O/F = 0.18:0.12:0.08:0.09:0.53 that is in reasonable relation with nominal G0-Rb_2KTiOF_5 composition Rb/K/Ti/O/F = 0.20:0.10:0.10:0.10:0.50. The Auger parameters of potassium, titanium, oxygen, and fluorine in G0-Rb_2KTiOF_5 are α_K = 542.7, α_{Ti} = 869.5, α_O = 1041.2, and α_F = 1340.2 eV.

Table 4. Constituent Element Core Levels and Auger Lines in G0-Rb_2KTiOF_5 and Related Compounds

Core level, Auger line	Binding energy, eV			
	G0-Rb_2KTiOF_5 (this work)	$K_3WO_3F_3$ [31]	$KTiOPO_4$ [51]	$RbTiOPO_4$ [52]
VB	3.8, 7.3			
Rb 4p	13.2			
K 3p	16.2	16.6		
O 2s	18.7	22.9		22.9
Rb 4s, F 2s	28.6	28.2 (F 2s)		28.2 (Rb 4s)
K 3s	32.4			
Ti 3p	37.6			36.8
Ti 3s	62.9			61.5
Rb 3d	109.4, 110.9			108.9, 109.9
Rb $3p_{3/2}$	237.7			237.1
Rb $3p_{1/2}$	246.6			246.0
C 1s	Fixed at 284.8	284.6	284.6	284.6
K $2p_{3/2}$	292.1	292.6	292.3	
K $2p_{1/2}$	289.1	295.4		
Rb 3s	321.1			320.4
K 2s	376.8	377.1		
Ti $2p_{3/2}$	459.2		458.4	458.6
Ti $2p_{1/2}$	464.8			464.2
O 1s	529.6	530.0	530.9	530.4
Ti 2s	565.3			564.9
F 1s	683.9	684.2		
F $KL_{23}L_{23}$	830.4, 833.5, 839.3, 847.8	830.0		
F KL_1L_{23}	856.6, 860.1	856.1		
F KL_1L_1	875.6			
O KLL	975.0, 995.4	975.8		976.2
Ti $L_3M_{23}M_{23}$	1070.4, 1076.3			1066.6, 1071.9, 1075.6
K $L_2M_{23}M_{23}$, $L_3M_{23}M_{23}$	1235.9, 1238.3	1235.7, 1237.9		
Rb Auger	1375.9, 1384.0			

The chemical bonding effects, appearing due to O/F anion complex in G0-Rb_2KTiOF_5, can be considered using constituent element core level parameters measured by XPS. Indeed, when metal interacts with fluorine, oxygen, or other anion forming elements, a redistribution of electron density occurs as a shift of valence electrons. This results in some variations of the electronic structure of inner shells of both the cations and anions, and the effect can be easily detected as a variation of the core level BE values. For example, BE (Ti $2p_{3/2}$) variation is as high as ~8 eV if we compare titanium metal and Na_2TiF_6.[37,53,54] However, for a selected chemical class of compounds, the effect is less pronounced and can be occasionally smashed by the surface charging effect typically observed for dielectric materials. The problem can be solved using the BE difference parameter that is more sensitive for chemical bonding analysis of dielectric crystals.[55−58] There is an additional benefit that the BE difference parameter is insensitive to BE scale calibration methods applied in different XPS spectrometers and wide comparison of earlier published results becomes possible.

The BE differences Δ(Rb−O) = BE (O 1s) − BE (Rb $3d_{5/2}$) and Δ(RB-F) = BE (F 1s) − BE (Rb $3d_{5/2}$) are suitable to be used for the characterization of Rb−O and Rb−F bonding. A valence electron shift from rubidium to anions decreases inner

dx.doi.org/10.1021/jp401391y | J. Phys. Chem. C 2013, 117, 7269−7278

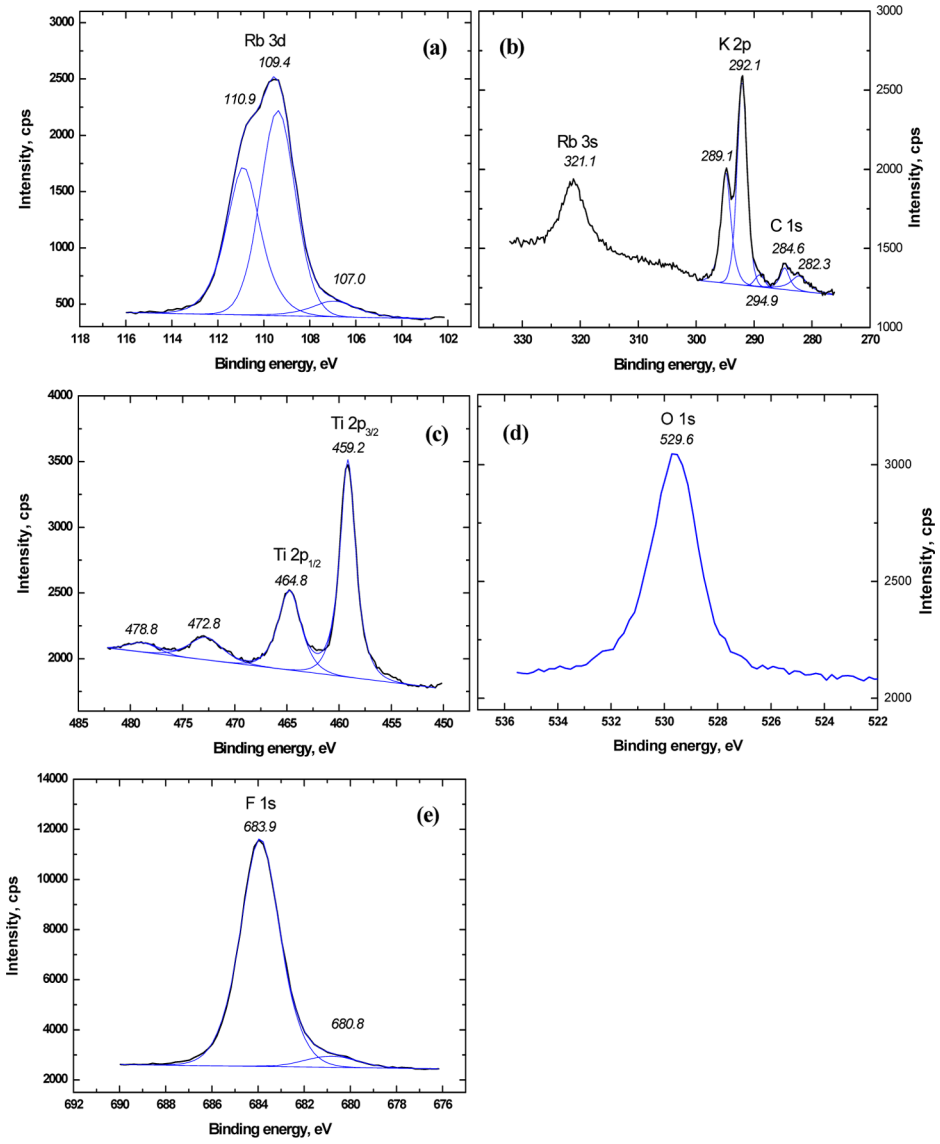

Figure 7. Detailed XPS spectrum of G0-Rb_2KTiOF_5. (a) Rb 3d doublet, (b) Rb 3s − K 2p − C 1s window, (c) Ti 2p doublet, (d) O 1s core level, (e) F 1s core level.

shell screening and induces an increase of BE (Rb $3d_{5/2}$) value. The values of BE (O 1s) or BE (F 1s) decrease in parallel. Thus, lower values of Δ(Rb−O) or Δ(Rb−F) indicate higher ionicity of Rb−O or Rb−F bonds. The collection of Rb-containing crystals measured by XPS is shown in Table 5. There is a difficulty in comparison because nearly a half of the compounds, including the key fluoride RbF, was measured by the spectrometer, where the components of Rb 3d doublet were not resolved. Nevertheless, as to oxides, the values of Δ(Rb−O) in different crystals are in the range of 420.3−421.5 eV with only one evident exception of $RbClO_4$, where the high measured BE(O 1s) seems to be drastically overestimated due to high hydrofility of the perchlorate surface.[59] The value of Δ(Rb−O) obtained from G0-Rb_2KTiOF_5 is at the lower boundary of range Δ(Rb−O) = 420.3−421.5 eV, and that indicates a very high ionicity of Rb−O bonds in this oxyfluoride. To compare the Rb−F bonding in RbF and G0-Rb_2KTiOF_5, the BE(Rb 3d) in the later compound can be roughly estimated by averaging the component values by relation BE(Rb 3d) ∼ (BE(Rb $3d_{5/2}$) + BE(Rb $3d_{3/2}$))/2 = 110.15 eV. So, in G0-Rb_2KTiOF_5, the value Δ(Rb−F) = 683.9 − 110.15 = 573.75 eV that is very close to the value calculated for RbF as Δ(Rb−F) = 683.8 − 110.0 = 573.8 eV.[59] So, the presence of a low oxygen component in G0-Rb_2KTiOF_5 at the level of O/F = 0.2 is of less influence on the Rb−F bonding. Contrary to that, high fluorine component seems to be able to provide higher-ionicity Rb−O bonds.

The representative suite of potassium-containing crystals is shown in Table 6. The BE differences Δ(K−F) = BE (F 1s) − BE (K $2p_{3/2}$) and Δ(K−O) = BE (O 1s) − BE (K $2p_{3/2}$) can be used for the characterization of K−F and K−O bonding, respectively. The range of Δ(K−F) = 390.5−392.4 eV is very wide in fluorides. Comparatively, the range Δ(K−F) = 391.6−392.0 eV defined in oxyfluorides is evidently narrower and Δ(K−F) = 391.8 eV obtained in G0-Rb_2KTiOF_5 is in the middle of the range. Thus, the ionicity of K−F bonds in G0-Rb_2KTiOF_5 is similar to that typical for complex fluorides and oxyfluorides. As to oxygen-containing crystals, the range Δ(K−O) = 237.6−238.6 eV found in oxides, excluding $KClO_4$ and $KClO_3$ where strong surface hydration is indicated by very high

dx.doi.org/10.1021/jp401391y | J. Phys. Chem. C 2013, 117, 7269−7278

Table 5. Core Level Parameters of Rb-Containing Crystals

compound	Rb 3d, Rb $3d_{5/2}$ (eV)	Rb $3p_{3/2}$ (eV)	O 1s (eV)	ΔBE(O − Rb) (eV)	ref
RbF	110.0[a]				59
RbCl	110.1[a]				59
RbBr	110.2[a]				59
$RbPb_2Br_5$	109.5	237.9			60
	109.20				61
$K_{0.5}Rb_{0.5}Pb_2Br_5$	109.22				61
RbI	110.6[a]				59
$RbClO_4$	110.6[a]		533.0	422.4	59
Rb_3PO_4	110.2[a]		530.5	420.3	59
$Rb_4P_2O_7$	110.2[a]		530.9	420.7	63
Rb_2SO_4	109.8		531.3	421.5	62
Rb_2CO_3	109.4		530.1	420.7	63
$RbHCO_3$	109.2		530.7	421.5	63
$Rb_2Sr(VO_3)_4$		237.8	530.2	292.4	64
$RbTiOPO_4$	~112.5[a]				65
$RbTiOPO_4$	108.9	237.1	530.4	421.5, 293.3	52
Rb_2KTiOF_5	109.4	237.7	529.6	420.2, 291.9	this study

[a]BE value is measured for Rb 3d band.

BE(O 1s) values, is similar to the range Δ(K−O) = 237.4−238.5 eV obtained in oxyfluorides. One can see value Δ(K−O) = 237.5 eV at the lower energy boundary of the ranges revealed in oxides and oxyfluorides that indicates the increased ionicity of K−O bonding in G0-Rb_2KTiOF_5.

A representative set of Ti-containing compounds is shown in Table 7 where BE differences Δ(Ti−O) = BE (O 1s) − BE (Ti $2p_{3/2}$) and Δ(Ti−F) = BE (F 1s) − BE (Ti $2p_{3/2}$) are applied as bonding-related parameters. The Ti−F and Ti−O bonds are partly covalent, and the effect of O/F ratio variation should be most pronounced. The variation of Δ(Ti−O) from 70.4 eV (G0-Rb_2KTiOF_5) to 71.26 eV (TiO_2) on the variation of O/F ratio from 0.2 to 1 is evident and that reveals the decreasing ionicity of Ti−O bonds. Contrary to that, the drastic decrease of Δ(Ti−F) parameter from 225.2 eV ($TiOF_2$) to 224.3 eV (TiF_4) is found with the decrease of O/F ratio from 0.33 to 0 that indicates the increasing ionicity of Ti−F bonds. Thus, the Ti-(O,F) bonding is very sensitive to the O/F ratio in oxyfluorides due to the competition of O^{2-} and F^- ions for the valence electrons provided by cations.

Figure 8b displays the first-principles electronic density of states (DOS) and partial DOS (PDOS) projected on the constituent atoms in Rb_2KTiOF_5. Compared to the experimental XPS spectrum (shown in Figure 8a), the Ti 3p orbitals are not displayed in the calculated PDOS, since these electrons are not treated as the valence electrons in our DFT calculations. The K 3s orbitals are quite localized at the very deep position in the valence band and have a small influence on the other

Table 6. Core Level Parameters of K-Containing Crystals

crystal	K $2p_{3/2}$	O 1s	F 1s	ΔBE(O − K) (eV)	ΔBE(F − K) (eV)	ref
KF	293.3		684.0		390.7	59
	294.0		684.5		390.5	70
K_2SiF_6	293.4		685.8		392.4	66
K_2GeF_6	293.1		685.4		392.3	66
K_2TiF_6	293.2		685.1		391.9	66
K_2ZrF_6	292.8		684.8		392.0	66
K_3ZrF_7	293.0		684.5		391.5	66
K_2NbF_7	293.5		685.4		391.9	66
K_2TaF_7	293.2		685.3		392.1	66
$KNiF_3$	293.15		685.1		392.0	67
$KZnF_3$	292.2		684.3		391.1	68
KPb_2Br_5	292.8					69
	292.62					61
$K_{0.5}Rb_{0.5}Pb_2Br_5$	292.56					61
$KClO_4$	293.6	532.4		238.8		59
$KClO_3$	293.4	532.5		239.1		59
K_3PO_4	292.7	530.6		237.9		59
$K_4P_2O_7$	292.4	530.3		237.9		59
K_2SO_4	293	531.6		238.6		62
K_2CO_3	292.2	530.2		238.0		63
$KHCO_3$	292.9	531.5		238.6		63
$KTiOPO_4$	292.3	530.9		238.6		51
$KTiOAsO_4$	292.8	531.2		238.4		71
$K_2Sr(VO_3)_4$	292.6	530.2		237.6		64
$KGd(WO_4)_2$	292.3	530.1		237.8		72
$KY(WO_4)_2$	292.7	530.8		238.1		73
KH_2PO_4	291.66	530.24		238.58		74
KWO_3F_3	292.6	530.0	684.2	237.4	391.6	31
K_3NbOF_6	293.1	531.6	685.1	238.5	392.0	66
K_2NbOF_5	293.4	531.8	685.4	238.4	392.0	66
$K_4Ta_4O_5F_{14}$	293.4	531.3	685.1	237.9	391.7	66
Rb_2KTiOF_5	292.1	529.6	683.9	237.5	391.8	this study

dx.doi.org/10.1021/jp401391y | J. Phys. Chem. C 2013, 117, 7269−7278

Table 7. Core Level Parameters of Ti-Containing Crystals

compound	Ti $2p_{3/2}$	O 1s	F 1s	ΔBE(O − Ti) (eV)	ΔBE(F − K) (eV)	ref
TiF_4	468.6[a]		692.8[b]		224.2	75
	461.3		685.7		224.4	76
$TiOF_2$	459.5	530.7	684.7	70.8	225.2	77
TiO_2	458.15	529.41		71.26		78
Rb_2KTiOF_5	459.2	529.6	683.9	70.4	224.7	this study

[a]Referenced to the N 1s level of N_2 (409.93 eV). [b]Referenced to the F 1s level of SF6 (695.04 eV).

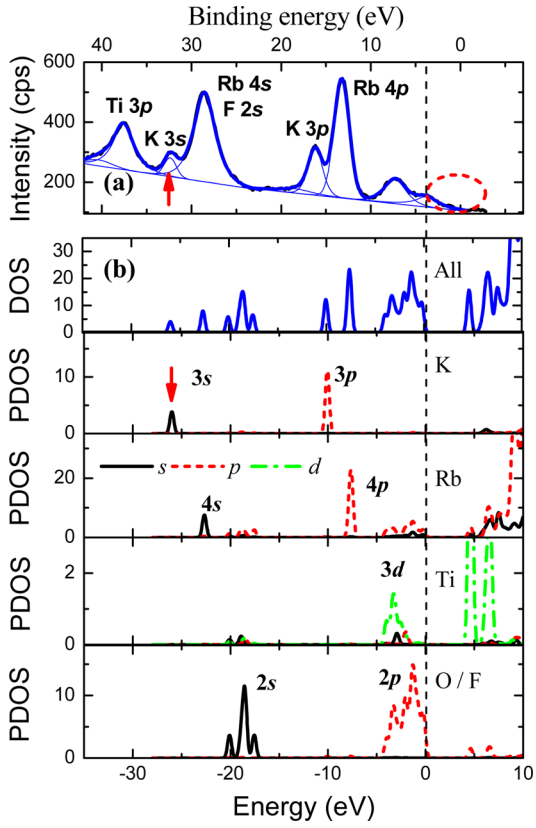

Figure 8. Comparison of (a) experimental XPS spectrum and (b) ab initio electronic structures. The vertical dashed line indicates the calculated valence band maximum, while red arrows indicate the alignment sites of the experimental and calculated peaks for K 3s orbtials.

orbitals. So this level is selected as the reference (indicated by red arrows in Figure 8) to align the experimental and calculated spectra. It is clear that the positions of the calculated Rb 4s, O/F 2s, K 3p and Rb 4p orbitals are in good agreements with the experimental measurements after the alignment, indicating the suitability of our calculated method for the Rb_2KTiOF_5 crystal. However, it should be noted that the electronic states indicated by the red dash circle (in Figure 8a) cannot be explained, and the O/F 2p and Ti 3d orbitals located at the top of calculated valence bands are not consistent with the experiments. It is argued that the top of the measured valence band spectrum is generated by the substrate which is not related to Rb_2KTiOF_5.

From the calculated PDOS, the chemical bonding characteristics in Rb_2KTiOF_5 can be deduced. The fact that K and Rb orbitals are deep in the valence band demonstrates that they form very weak bonds with the neighboring atoms. As a comparison, the upper valence states from −5 eV to the valence band maximum are mainly contributed to from Ti and O/F atoms and show quite a large hybridization between Ti 3d and O/F 2p states, manifesting the strong covalent bonds formed between the Ti−O/F ions. At the same time, the conduction band minimum exhibits the main contribution from Ti orbitals, which means that the energy band gap in Rb_2KTiOF_5 is determined by the electron transition inside the Ti−O/F groups.

5. CONCLUSIONS

In the present study, the spectroscopic and electronic parameters of Rb_2KTiOF_5 oxyfluoride were evaluated for the first time. The preparation of nearly a centimeter-sized single crystal permits to the measurement of the transparency range and the determination of the optical band gap in Rb_2KTiOF_5. Strong and broad-band luminescence was found in Rb_2KTiOF_5 under excitation in UV and the visible spectral ranges, PL bands at 3.36 and 2.33 eV are related to free and self-trapped excitons, respectively. Electronic structure observation shows interesting chemical bonding effects appeared due to the presence of O/F anion complex in the crystal lattice. As the result of a wide comparison of BE values of representative core levels measured by XPS in Rb_2KTiOF_5 and other oxides, fluorides and oxyfluorides containing Rb^+, K^+, and Ti^{4+} cations, it is found that cation−anion bond ionicity is noticeably dependent on the O/F ratio in oxyfluorides. The most pronounced effect is detected for Ti−O/F bonding, where bonds are of partly covalent character. Previously, similar effects were found for Cs^+, Mn^{2+}, and Mo^{6+} ions in $CsMnMoO_3F_3$ oxyfluoride.[32] Thus, the variation of bond ionicity due to the competition of O^{2-} and F^- ions for the valence electrons provided by metals seems to be a general phenomenon in oxyfluorides. If this is the case, the earlier created systems of effective ionic radii in oxides and fluorides may be not correct in oxyfluorides and the creation of developed radii systems is topical, for which the dependence of effective ionic radii on the O/F ratio is accounted.[48,79,80]

AUTHOR INFORMATION

Corresponding Author

*Tel.: 86-10-82543718. E-mail: zslin@mail.ipc.ac.cn.

Notes

The authors declare no competing financial interest.

ACKNOWLEDGMENTS

This study was supported by SB RAS (Grant 28.13), the National Natural Science Foundation of China under Grants 11174297 and 91022036, and the National Basic Research Project of China (Nos. 2010CB630701 and 2011CB922204).

REFERENCES

(1) Pausewang, G.; Rüdorff, W. $A_3^IMeO_xF_{6-x}$-Verbindungen Mit x = 1,2,3. *Z. Anorg. Allg. Chem.* **1969**, *364*, 69−87.

(2) Dehnicke, K.; Pausewang, G.; Rüdorff, W. Die IR-Spectren der Oxofluorokomplexe $TiOF_5^{3-}$, VOF_5^{3-}, $NbO_2F_4^{3-}$, $MoO_3F_3^{3-}$ und $WO_3F_3^{3-}$. *Z. Anorg. Allg. Chem.* **1969**, *366*, 64−72.
(3) Ravez, J.; Peraudeau, G.; Arend, H.; Abrahams, S. C.; Hagenmuller, P. A New Family of Ferroelectric Materials with Composition $A_2BMO_3F_3$ (A, B = K, Rb, Cs, for $r_{A+} \geq r_{B+}$ and M = Mo, W). *Ferroelectrics* **1980**, *26*, 767−769.
(4) Grannec, J.; Yacoubi, A.; Linke, D.; Tressaud, A.; Hagenmuller, P. Phase Transitions and Some Physical Properties in Fluorides and Oxide Fluorides Containing Monovalent Silver. *J. Fluorine Chem.* **1985**, *29* (1−2), 59.
(5) Marvel, M. R.; Lesage, J.; Baek, J.; Halasyamani, P. S.; Stern, C. L.; Poeppelmeier, K. R. Cation−Anion Interaction and Polar Structures in the Solid State. *J. Am. Chem. Soc.* **2007**, *129*, 13963−13969.
(6) Marvel, M. R.; Pinlac, R. A. F.; Lesage, J.; Stern, C. L.; Poeppelmeier, K. R. Chemical Hardness and the Adaptive Coordination Behavior of the d^0 Transition Metal Oxide Fluoride Anions. *Z. Anorg. Allg. Chem.* **2009**, *635*, 869−877.
(7) Flerov, I. N.; Gorev, M. V.; Tressaud, A.; Laptash, N. M. Perovskite-like Fluorides and Oxyfluorides: Phase Transitions and Caloric Effects. *Cryst. Rep.* **2011**, *56* (1), 9−17.
(8) Peraudeau, G.; Ravez, J.; Hagenmuller, P. Study of Phase Transitions in $A_3MO_3F_3$ Compounds (A = K, Rb, Cs; M = Mo, W). *Solid State Commun.* **1978**, *27*, 591−593.
(9) Flerov, I. N.; Fokina, V. D.; Gorev, M. V.; Vasiliev, A. D.; Bovina, A. F.; Molokeev, M. S.; Kocharova, A. G.; Laptash, N. M. Mechanism of Phase Transitions in the $(NH_4)_2WO_2F_4$ Ferroelastic. *Phys. Solid State* **2006**, *48* (4), 759−764.
(10) Flerov, I. N.; Gorev, M. V.; Fokina, V. D.; Molokeev, M. S. Phase Transitions in Oxides, Fluorides and Oxyfluorides with the Ordered Perovskite Structure. *Ferroelectrics* **2007**, *346*, 77−83.
(11) Molokeev, M. S.; Misyul, S. V.; Fokina, V. D.; Kocharova, A. G.; Aleksandrov, K. S. Structure Transformations during Phase Transitions in the $K_3WO_3F_3$ Oxyfluoride. *Phys. Solid State* **2011**, *53*, 834−839.
(12) Abrahams, S. C.; Bernstein, J. L. Paraelectric-paraelastic $Rb_2KMoO_3F_3$ Structure at 343 and 473 K. *Acta Cryst. B* **1981**, *37*, 1332−1336.
(13) Mel'nikova, S. V.; Fokina, V. D.; Laptash, N. M. Phase Transitions in Oxyfluoride $(NH_4)_2WO_2F_4$. *Phys. Solid State* **2006**, *48*, 117−121.
(14) Gorev, M.; Bogdanov, E.; Flerov, I.; Laptash, N. Thermal Expansion, Phase Diagrams and Barocaloric Effects in $(NH_4)_2NbOF_5$. *J. Phys.: Condens. Matter* **2010**, *22*, 185901.
(15) Melnikova, S. V.; Laptash, N. M.; Aleksandrov, K. S. Optical Studies of Phase Transitions in Oxyfluoride $(NH_4)_2NbOF_5$. *Phys. Solid State* **2010**, *52*, 2168−2172.
(16) Chamberlain, J. M.; Albrecht, T. A.; Lesage, J.; Sauvage, F.; Stern, C. L.; Poeppelmeier, K. R. Crystal Growth of $Ag_3Mo_xF_{6-x}$ (M = V, x = 2; M = Mo, x = 3). *Cryst. Growth Des.* **2010**, *10*, 4868−4873.
(17) Kartashev, A. V.; Molokeev, M. S.; Isaenko, L. I.; Zhurkov, S. A.; Fokina, V. D.; Gorev, M. V.; Flerov, I. N. Heat Capacity and Structure of $Rb_2KMeO_3F_3$ (Me: Mo, W) Elpasolites. *Solid State Sci.* **2012**, *14*, 166−170.
(18) Atuchin, V. V.; Isaenko, L. I.; Kesler, V. G.; Lin, Z. S.; Molokeev, M. S.; Yelisseyev, A. P.; Zhurkov, S. A. Exploration on Anion Ordering, Optical Properties and Electronic Structure in $K_3WO_3F_3$ Elpasolite. *J. Solid State Chem.* **2012**, *187*, 159−164.
(19) Krylov, A. S.; Merkushova, E. M.; Vtyurin, A. N.; Isaenko, L. I. Raman Spectroscopic Study of the Lattice Dynamics in the $Rb_2KMoO_3F_3$ Oxyfluoride. *Phys. Solid State* **2012**, *54*, 1275−1280.
(20) Bogdanov, E. V.; Pogoreltsev, E. I.; Mel'nikova, S. V.; Gorev, M. V.; Flerov, I. N.; Molokeev, M. S.; Kartashev, A. V.; Kocharova, A. G.; Laptash, N. M. Investigation Into Phase Diagrams of the Fluorine-oxygen System: Ferroeleastic-antiferroelastic $(NH_4)_2WO_2F_4$-$(NH_4)_2MoO_2F_4$. *Phys. Solid State* **2013**, *55*, 409−418.
(21) Sorokina, N. I.; Voronkova, V. I. Structure and Properties of Crystals in the Potassium Titanyl Phosphate Family: A Review. *Cryst. Reports* **2007**, *52*, 80−93.
(22) Fokina, V. D.; Flerov, I. N.; Molokeev, M. S.; Pogorel'tsev, E. I.; Bogdanov, E. V.; Krylov, A. S.; Bovina, A. F.; Voronov, V. N.; Laptash, N. M. Heat Capacity, p-T Phase Diagram, and Structure of Rb_2KTiOF_5. *Phys. Solid State* **2008**, *50*, 2175−2183.
(23) Udovenko, A. A.; Laptash, N. M. Dynamic Orientational Disorder in Crystals of Fluoroelpasolites, Structural Refinement of $(NH_4)_3AlF_6$, $(NH_4)_3TiOF_5$ and Rb_2KTiOF_5. *Acta Cryst. B* **2011**, *67*, 447−454.
(24) Gorev, M. V.; Flerov, I. N.; Bogdanov, E. V.; Voronov, V. N.; Laptash, N. M. Barocaloric Effect Near the Structural Phase Transition in the Rb_2KTiOF_5 Oxyfluoride. *Phys. Solid State* **2010**, *52*, 377−383.
(25) Gorev, M. V.; Bogdanov, E. V.; Flerov, I. N.; Voronov, V. N.; Laptash, N. M. Barocaloric Effect in Oxyfluorides Rb_2KTiOF_5 and $(NH_4)_2NbOF_5$. *Ferroelectrics* **2010**, *397*, 76−80.
(26) Aleksandrov, K. S.; Anistratov, A. T.; Besnosikov, B. V.; Fedoseeva, N. V. *Phase transitions in hallide crystals ABX_3*; Nauka: Novosibirsk, 1981; p 264.
(27) Flerov, I. N.; Gorev, M. V.; Aleksandrov, K. S.; Tressaud, A.; Grannec, J.; Couzi, M. Phase transitions in elpasolities (ordered perovskites). *Mater. Sci. Eng. R* **1998**, *24*, 81−151.
(28) Voit, E. I.; Davydov, V. A.; Mashkovskii, A. A.; Voit, A. V. Investigation of Oxofluorotitanates $(NH_4)_3TiOF_5$ and Rb_2KTiOF_5 by Vibrational Spectroscopy and Quantum-chemical Methods. *J. Struct. Chem.* **2008**, *49*, 13−20.
(29) Kavun, V. Ya.; Kozlova, S. G.; Tkachenko, I. A.; Gabuda, S. P. NMR and DFT Study of Chemical Bonding in the Titanyl Ion in Pentafluoro Complaxes $(NH_4)_3TiOF_5$ and Rb_2KTiOF_5. *J. Struct. Chem.* **2010**, *51*, 463−470.
(30) Krylov, A. S.; Goryainov, S. V.; Vtyurin, A. N.; Krylova, S. N.; Sofronova, S. N.; Laptash, N. M.; Emelina, T. B.; Voronov, V. N.; Babushkin, S. V. Raman Scattering Study of Temperature and Hydrostatic Pressure Phase Transitions in Rb_2KTiOF_5 Crystal. *J. Raman Spectrosc.* **2012**, *43*, 577−582.
(31) Atuchin, V. V.; Gavrilova, T. A.; Kesler, V. G.; Molokeev, M. S.; Aleksandrov, K. S. Structural and Electronic Parameters of Ferroelectric $K_3WO_3F_3$. *Solid State Commun.* **2010**, *150*, 2085−2088.
(32) Atuchin, V. V.; Molokeev, M. S.; Yurkin, G. Yu.; Gavrilova, T. A.; Kesler, V. G.; Laptash, N. M.; Flerov, I. N.; Patrin, G. S. Synthesis, Structural, Magnetic, and Electronic Properties of Cubic $CsMnMoO_3F_3$ Oxyfluoride. *J. Phys. Chem. C* **2012**, *116*, 10162−10170.
(33) Atuchin, V. V.; Gavrilova, T. A.; Isaenko, L. I.; Kesler, V. G.; Molokeev, M. S.; Zhurkov, S. A. Synthesis and Structural Properties of Cubic G0-$Rb_2KMoO_3F_3$ Oxyfluoride. *Ceram. Int.* **2012**, *38*, 2455−2459.
(34) Sheldrick, G. M. Phase Annealing in Shelx-90: Direct Methods for Lager Structures. *Acta Cryst. A* **1990**, *46*, 467−473.
(35) Sheldrick, G. M. *Shelxl−97: A Computer Program for Refinement of Crystal Structures*, University of Göttingen: Germany.
(36) Moss, T. S. *Optical Properties of Semiconductors*; Butterworth: London, 1961.
(37) Handbook of X-ray Photoelectron Spectroscopy; Wagner, C. D., Riggs, W. M., Davis, L. E., Moulder, J. F., Muilenberg, G. E., Eds.; Perkin-Elmer Corp., Physical Electronics. Division: Eden Prairie, Minnesota, 1979.
(38) Payne, M. C.; Teter, M. P.; Allan, D. C.; Arias, T. A.; Joannopoulos, J. D. Iterative Minimization Techniques for Ab Initio Total-energy Calculations - Molecular-dynamics and Conjugate Gradients. *Rev. Mod. Phys.* **1992**, *64*, 1045−1097.
(39) Clark, S. J.; Segall, M. D.; Pickard, C. J.; Hasnip, P. J.; Probert, M. J.; Refson, K.; Payne, M. C. First Principles Methods Using CASTEP. *Z. Krystallogr.* **2005**, *220*, 567−570.
(40) Kohn, W.; Sham, L. J. Self-Consistent Equations Including Exchange and Correlation Effects. *Phys. Rev. A* **1965**, *140*, 1133−&.
(41) Rappe, A. M.; Rabe, K. M.; Kaxiras, E.; Joannopoulos, J. D. Optimized Pseudopotentials. *Phys. Rev. B* **1990**, *41*, 1227−1230.

(42) Lin, J. S.; Qtseish, A.; Payne, M. C.; Heine, V. Optimized and Transferable Nonlocal Separable Ab Initio Pseudopotentials. *Phys. Rev. B* **1993**, *47*, 4174−4180.
(43) Perdew, J. P.; Burke, K.; Ernzerhof, M. Generalized Gradient Approximation Made Simple. *Phys. Rev. Lett.* **1996**, *77*, 3865−3868.
(44) Perdew, J. P.; Wang, Y. Accurate and Simple Analytic Representation of the Electron-gas Correlation-energy. *Phys. Rev. B* **1992**, *45*, 13244−13249.
(45) Monkhors, H. J.; Pack, J. D. Special Points for Brillouin-zone Integrations. *Phys. Rev. B* **1976**, *13*, 5188−5192.
(46) Bellaiche, L.; Vanderbilt, D. Virtual Crystal Approximation Revisited: Application to Dielectric and Piezoelectric Properties of Perovskites. *Phys. Rev. B* **2000**, *61*, 7877−7882.
(47) Ozawa, T. C.; Kang, S. J. Balls & Sticks: Easy-to-use Structure Vizualization and Animation Program. *J. Appl. Crystallogr.* **2004**, *37*, 679.
(48) Prince, E. *International Tables for Crystallography. C (Mathematical, Physical and Chemical Tables)*, 3rd ed.; Kluver Academic Publishers: Dordrecht, 2004; p 1000.
(49) Yelisseyev, A. P.; Starikova, M. K.; Korolev, V. V.; Isaenko, L. I.; Lobanov, S. I. Photoluminescence of lithium thiogallate $LiGaS_2$. *J. Opt. Soc. Am. B* **2012**, *29*, 1003−1011.
(50) Song, K. S.; Williams, R. T. *Self-trapped excitons*; Springer Verlag, Berlin, 1993; Vol. *XII*, p 403.
(51) Atuchin, V. V.; Kesler, V. G.; Maklakova, N.Yu.; Pokrovsky, L. D.; Semenenko, V. N. Study of $KTiOPO_4$ Surface by X-ray Photoelectron Spectroscopy and Reflection High-Energy Electron Diffraction. *Surf. Interface Anal.* **2002**, *34*, 320−323.
(52) Atuchin, V. V.; Kesler, V. G.; Meng, G. S.; Lin, Z. S. The Electronic Structure of $RbTiOPO_4$ and the Effects of the A-site Cation Substitution in $KTiOPO_4$-family Crystals. *J. Phys.: Condens. Matter* **2012**, *24*, 405503.
(53) Nefedov, V. I. *X-ray photoelectron spectroscopy of chemical compounds: Handbook*; Khimia: Moscow, 1984.
(54) Barr, T. L. Recent Advances in X-ray Photoelectron Spectroscopy Studies of Oxides. *J. Vac. Sci. Technol., A* **1991**, *9*, 1793−1805.
(55) Atuchin, V. V.; Kalabin, I. E.; Kesler, V. G.; Pervukhina, N. V. Nb 3d and O 1s Core Levels and Chemical Bonding in Niobates. *J. Electron Spectrosc. Relat. Phenom.* **2006**, *142*, 129−134.
(56) Atuchin, V. V.; Kesler, V. G.; Pervukhina, N. V.; Zhang, Z. M. Ti 2p and O 1s Core Levels and Chemical Bonding in Titanium-bearing Oxides. *J. Electron Spectrosc. Relat. Phenom.* **2006**, *152*, 18−24.
(57) Atuchin, V. V.; Kesler, V. G.; Pervukhina, N. V. Electronic and Structural Parameters of Phosphorus-oxygen Bonds in Inorganic Phosphate Crystals. *Surf. Rev. Lett.* **2008**, *15*, 391−399.
(58) Atuchin, V. V.; Galashov, E. N.; Khyzhun, O.Yu.; Kozhukhov, A. S.; Pokrovsky, L. D.; Shlegel, V. N. Structural and Electronic Properties of $ZnWO_4$(010) Cleaved Surface. *Cryst. Growth Des.* **2011**, *11*, 2479−2484.
(59) Morgan, W. E.; Van Wazer, J. R.; Stec, W. J. Inner-Orbital Photoelectron Spectroscopy of the Alkali Metal Halides, Perchlorates, Phosphates, and Pyrophosphates. *J. Am. Chem. Soc.* **1973**, *95*, 751−755.
(60) Atuchin, V. V.; Isaenko, L. I.; Kesler, V. G.; Pokrovsky, L. D.; Tarasova, A.Yu. Electronic Parameters and Top Surface Chemical Stability of $RbPb_2Br_5$. *Mater. Chem. Phys.* **2012**, *132*, 82−86.
(61) Tarasova, A.Yu.; Isaenko, L. I.; Kesler, V. G.; Pashkov, V. M.; Yelisseyev, A. P.; Denysyuk, N. M.; Khyzhun, O.Yu. Electronic Structure and Fundamental Absorption Edges of KPb_2Br_5, $K_{0.5}Rb_{0.5}Pb_2Br_5$, and $RbPb_2Br_5$ Single Crystals. *J. Phys. Chem. Solids* **2012**, *73*, 674−682.
(62) Wahlqvist, M.; Shchukarev, A. XPS Spectra and Electronic Structure of Group IA Sulfates. *J. Electron Spectrosc. Relat. Phenom.* **2007**, *156−158*, 310−314.
(63) Shchukarev, A. V.; Korolkov, D. V. XPS Study of Group IA Carbonates. *Central Europ. J. Chem.* **2004**, *2*, 347−362.
(64) Slobodin, B. V.; Sarat, L. L.; Zubkov, V. G.; Tyutyunnik, A. P.; Berger, I. F.; Kuznetsov, M. V.; Perelyaeva, L. A.; Shein, I. R.; Ivanovskii, A. L.; Shulgin, B. V.; et al. Structural, Luminescence, and Electronic Properties of the Alkaline Metal-strontium Cyclotetravanadates $M_2Sr(VO_3)_4$. *Phys. Rev. B* **2005**, *72*, 155205.
(65) Liu, Z. G.; Liu, J. M.; Ming, N. B.; Wang, J. Y.; Liu, Y. G.; Jiang, M. H. Epitaxial Growth of $RbTiOPO_4$ Films on $KTiOPO_4$ Substrates by Excimer Laser Ablation Technique. *J. Appl. Phys.* **1994**, *76*, 8215−8217.
(66) Zhavoronkov, N. M.; Nefedov, V. I.; Buslaev, Yu. A.; Kokunov, Yu. V.; Porai-Koshits, M. A.; Ilin, E. G.; Mihailov, Yu. N. XPS Study of Complex Fluorides and Oxyfluorides of Elements from IV-VI Groups. *Izv. Akad. Nauk USSR, Physics* **1972**, *36*, 376−380.
(67) Zhang, M.; Wang, Z. H.; Mo, M. S.; Chen, X. Y.; Zhang, R.; Yu, W. C.; Qian, Y. T. A Simple Approach to Synthesize $KNiF_3$ Hollow Spheres by Solvothermal Method. *Mater. Chem. Phys.* **2005**, *89*, 373−378.
(68) Huang, B.; Hong, J. M.; Chen, X. T.; Yu, Z.; You, X. Z. Mild Solvothermal Synthesis of $KZnF_3$ and $KCdF_3$ Nanocrystals. *Mater. Lett.* **2005**, *59*, 430−433.
(69) Atuchin, V. V.; Isaenko, L. I.; Kesler, V. G.; Tarasova, A. Yu. Single Crystal Growth and Surface Chemical Stability of KPb_2Br_5. *J. Cryst. Growth* **2011**, *318*, 1000−1004.
(70) Nemoshkalenko, V. V.; Senkevich, A. I.; Aleshin, V. G. Photoelectron Spectra and Band Structure of Alkali Hallide Crystals. *Dokl. Akad. Nauk USSR* **1972**, *206*, 593−596.
(71) Atuchin, V. V.; Isaenko, L. I.; Khyzhun, O.Yu.; Pokrovsky, L. D.; Sinelnichenko, A. K.; Zhurkov, S. A. Structural and Electronic Properties of the $KTiAsO_4$(001) Surface. *Opt. Mater.* **2008**, *30*, 1149−1152.
(72) Atuchin, V. V.; Kesler, V. G.; Maklakova, N. Yu.; Pokrovsky, L. D. Core Level Spectroscopy and RHEED Analysis of $KGd(WO_4)_2$ Surface. *Solid State Commun.* **2005**, *133*, 347−351.
(73) Atuchin, V. V.; Pokrovsky, L. D.; Khyzhun, O.Yu.; Sinelnichenko, A. K.; Ramana, C. V. Surface Crystallography and Electronic Structure of Potassium Yttrium Tungstate. *J. Appl. Phys.* **2008**, *104*, 033518.
(74) Engelhard, M.; Evans, C.; Land, T. A.; Nelson, A. Study of Potassium Dihydrogen Phosphate (KDP) Crystal Surfaces by XPS. A.J. *Surf. Sci. Spectra* **2001**, *8*, 56−80.
(75) Wallbank, B.; Perera, J. S. H. Q.; Frost, D. C.; McDowell, C. A. X-ray Photoelectron Spectroscopy of Titanium Tetrahalide Vapors. *J. Chem. Phys.* **1978**, *69*, 5405−5410.
(76) Klimov, V. D.; Vashman, A. A.; Pronin, I. S. Study of Atomic Titanium Interaction with PF_3 Matrix at 77 K − Cryochemical Synthesis of $TiF_2{\cdot}PF_3$ Monotriphosphinetitanium (II) Fluoride New Compounds. *Zh. Obshch. Khim.* **1991**, *61*, 2166−2174.
(77) Wen, C. Z.; Hu, Q. H.; Guo, Y. N.; Gong, X. Q.; Qiao, S. Z.; Yang, H. G. From Titanium Oxyfluoride ($TiOF_2$) to Titania (TiO_2): Phase Transition and Non-metal Doping with Enhanced Photocatalytic Hydrogen (H_2) Evolution Properties. *Chem. Commun.* **2011**, *47*, 6138−6140.
(78) Silversmit, G.; De Doncker, G.; De Gryse, R. A Mineral TiO_2 (001) Anatase Crystal Examined by XPS. *Surf. Sci. Spectra* **2002**, *9*, 21−29.
(79) Shannon, R. D.; Prewitt, C. T. Effective Ionic Radii in Oxides and Fluorides. *Acta Cryst. B* **1969**, *25*, 925−946.
(80) Shannon, R. D. Revised Effective Ionic Radii and Systematic Studies of Interatomic Distances in Halides and Chalcogenides. *Acta Cryst. A* **1976**, *32*, 751−767.